Almost Isotropic Perimeters in Topology Optimization: Theoretical and Numerical Aspects

J. Petersson
Linköping University, Sweden
M. Beckers and P. Duysinx
University of Liège, Belgium

1. Abstract
We consider topology optimization of elastic continuum structures including a bound on the perimeter of the structure's domain. Such a bound is known to ensure existence of solutions and it stabilizes the behavior of numerical finite element (FE) solutions. However, the straightforward way of calculating the perimeter is *rotationally mesh-dependent*. In this paper we present new perimeter formulae with weaker rotational dependence, i.e. perimeters that are "almost isotropic". An overview of some theoretical results as well as numerical tests are given.

2. Keywords
Topology Optimization, Finite Elements, Perimeter Constraints

3. Problem Formulation
The considered optimization problem is concerned with designing shapes, holes and connectivities of a structure contained in a given open domain $\Omega \subset \mathbb{R}^d$ to achieve maximum stiffness with respect to given boundary conditions. Each point $\mathbf{x} \in \Omega$ is assigned a displacement $\mathbf{u}(\mathbf{x})$ and an amount of material $\rho(\mathbf{x})$. For fixed ρ we denote by $a(\rho,\cdot,\cdot)$ the internal work symmetric bilinear form and $\ell(\cdot)$ the external load linear form. Then the design problem can be written as

$$(\mathbb{P}) \quad \begin{cases} \text{Minimize} & \ell(\mathbf{u}) \quad \textit{(compliance)} \\ \rho,\ \mathbf{u} \in \mathbf{V} & \\ \text{subject to:} & a(\rho,\mathbf{u},\mathbf{v}) = \ell(\mathbf{v}), \quad \text{for all } \mathbf{v} \in \mathbf{V}, \\ & \int_\Omega \rho\, dx \le \overline{V}, \quad TV(\rho) \le \overline{P}, \quad \rho(\mathbf{x}) \in \{\underline{\rho},\overline{\rho}\} \quad \text{a.e. in } \Omega \end{cases}$$

in which $\overline{\rho}$ signifies the ρ-value for full material and $\underline{\rho}$ signifies void[1]. The first constraint is the *principle of virtual work* for the structure with material distribution ρ. The last line of $(\mathbb{P})$ represents the *design constraints*. The problem $(\mathbb{P})$ can be understood as optimizing over all measurable subsets of Ω with volume (area) bounded by $\overline{V}$ and perimeter not greater than $\overline{P}$. To bound the perimeter, i.e. the "total variation" (TV) of ρ, was introduced in topology optimization by Haber et al. [1] and then further developed by Beckers (e.g. [2]) and Duysinx (e.g. [3]). This bound will ensure existence of solutions [4] and consequently one obtains numerical FE solutions that are convergent with mesh-refinement [5]. This means that one achieves reliable values for displacements and stresses by refining the mesh, since poorly approximated structural parts (e.g. "bars" with maybe only one or two FE's width) will not split up into several poorly approximated parts as a finer mesh is utilized. Moreover, for basically any choice of FEs, formations of checkerboard patterns in the design picture will disappear for sufficiently refined grids [5].

4. Some Theory on TV-measures
The *total variation* in Ω of a function $\rho \in L^1(\Omega)$ is defined as

$$TV(\rho) = \sup_{\boldsymbol{\varphi}} \left\{ \int_\Omega \rho \operatorname{div} \boldsymbol{\varphi} \;\middle|\; \boldsymbol{\varphi} \in \mathbf{C}_0^1(\Omega), \quad \boldsymbol{\varphi}(\mathbf{x}) \in B(1) \quad \forall \mathbf{x} \in \Omega \right\} \tag{1}$$

where $B(r)$ is the closed ball in $\mathbb{R}^d$ with radius r, and the *perimeter* of a measurable set Ω_S in Ω is defined as $P(\Omega_S) = TV(\chi_{\Omega_S})$. In a measure-theoretical sense one has $P(\Omega_S) = |\partial\Omega_S \cap \Omega|$ where $|\cdot|$ denotes the $(d-1)$-dimensional Hausdorff measure.

Using (1) on FE-approximated functions, such as piecewise constants, actually results in numerical solutions that approach exact solutions to a version of $(\mathbb{P})$ where TV has to be replaced by a "taxi-cab" perimeter [5,6]. When $d = 2$ this perimeter equals the sum of the structure's edge lengths projected onto the coordinate axes. Hence this version of $(\mathbb{P})$ and its FE-approximations are formulated in terms of *frame-dependent* and *rotationally mesh-dependent* perimeters respectively. In order to reduce this dependence we will present TV-measures similar to what has been proposed in image segmentation [7].

[1] In general it will be necessary to avoid singularities by setting $\underline{\rho} > 0$, which means that structural holes are modelled with a *very compliant material*.

The *taxi-cab total variation* introduced in [5] is denoted TV_2 and is defined by (1) with $B(1)$ replaced by $Q(1)$ where $Q(r)$ is the closed d-cell with side length $2r$. Assume that $d = 2$ and ρ is smooth. Then

$$TV(\rho) = \int_\Omega |\nabla \rho| \; dx \text{ and } TV_2(\rho) = \int_\Omega \left(|\frac{\partial \rho}{\partial x_1}| + |\frac{\partial \rho}{\partial x_2}| \right) \; dx. \tag{2}$$

The second of (2) can be interpreted as computing the sum of the variation of ρ in the two directions $\mathbf{e}_{x_1}$ and $\mathbf{e}_{x_2}$. We now generalize this to more than two directions. Given a set of directions $\{\mathbf{e}_1, \ldots, \mathbf{e}_m\}$ where $\mathbf{e}_i = \cos\alpha_i \mathbf{e}_{x_1} + \sin\alpha_i \mathbf{e}_{x_2}$, $0 \le \alpha_i < \pi$, define a multidirectional measure

$$TV_m(\rho) = c_m \sum_{i=1}^{m} \int_\Omega |\nabla \rho \cdot \mathbf{e}_i| \, dx, \quad \text{where e.g.} \quad c_m^{-1} = \sum_{i=1}^{m} |\cos\alpha_i|. \tag{3}$$

Let $\boldsymbol{\alpha}$ denote the vector of the angles α_i. Choosing $\boldsymbol{\alpha}^T = (\, 0 \,,\, \pi/2 \,)$ the general definition (3) reduces to the second of (2) for $m = 2$. Let κ be a positive number and define the angles γ, θ and δ through $\tan\gamma = \kappa/2$, $\tan\theta = \kappa$ and $\tan\delta = 2\kappa$. We now also choose

$$\boldsymbol{\alpha}^T = (\, 0 \,,\, \theta \,,\, \pi/2 \,,\, \pi - \theta \,) \text{ for } m = 4, \text{ and } \quad \boldsymbol{\alpha}^T = (\, 0 \,,\, \gamma \,,\, \theta \,,\, \delta \,,\, \pi/2 \,,\, \pi - \delta \,,\, \pi - \theta \,,\, \pi - \gamma \,) \text{ for } m = 8.$$

It then follows that $c_4^{-1} = 1 + 2\,|\cos\theta|$ and $c_8^{-1} = 1 + 2\,|\cos\theta| + 2\,|\cos\gamma| + 2\,|\cos\delta|$.

To illustrate the properties of these multidirectional measures, let the function ρ_β be such that $\nabla\rho_\beta = \cos\beta \mathbf{e}_{x_1} + \sin\beta \mathbf{e}_{x_2}$, take $\kappa = 1$ and $|\Omega| = 1$. Then $TV(\rho_\beta) = 1$ for all β, but for the other measures one has $TV_m(\rho_\beta) = c_m \sum_{i=1}^{m} |\cos(\alpha_i - \beta)|$, cf. Fig. 1. This picture indicates how the length of a structural edge — in the new multidirectional measures — will depend on the rotation. The maximum value is $\sqrt{2}$ for TV_2,

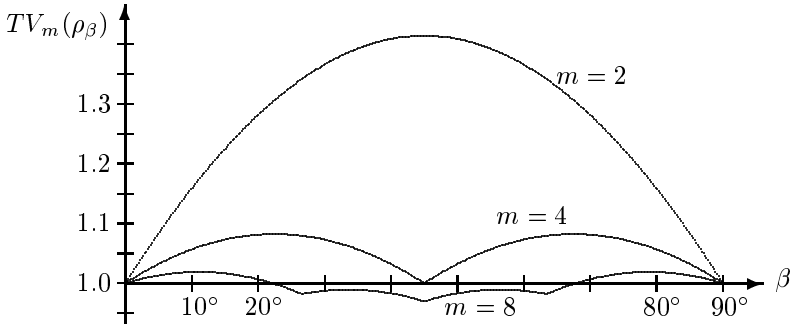

Figure 1: $TV_m(\rho_\beta)$ as a function of β for $m = 2, 4, 8$.

$(\sqrt{4+2\sqrt{2}})/(1+\sqrt{2}) \approx 1.0824$ for TV_4, and ≈ 1.01906 for TV_8. The minimum value for TV_8 is ≈ 0.969895. The "degree of anisotropy", based on the ratio between the largest and smallest value, is hence about 41.4% for TV_2, 8.24% for TV_4, and 5.06% for TV_8.

Assume that a rectangular domain $\Omega \subset \mathbb{R}^2$ is partitioned into a uniform mesh of $m = (n_1 + 1)(n_2 + 1)$ rectangles of equal size, i.e., $n_1 + 1$ finite elements in the horizontal direction and $n_2 + 1$ in the vertical. All edges of the elements Ω_{ij} are parallel to the coordinate axes, and the element width is h_1 and the height is h_2. Let Π_h be an operator which gives the elementwise constant interpolation such that the value of $\Pi_h\rho$ in Ω_{ij} is the integral mean of ρ over Ω_{ij}.

A crucial point for FE-solutions to really approximate exact ones, is that the interpolant should remain in the proper set, e.g. if a continuous displacement $\mathbf{u} \in \mathbf{V} \subset \mathbf{H}^1(\Omega)$, then the piecewise linear interpolant $\pi_h\mathbf{u}$ belongs to $\mathbf{V}$. For ρ this means that $TV(\rho) \le c$ should imply $TV(\Pi_h\rho) \le c$. However, by considering e.g. an edge which is parallel to neither $\mathbf{e}_{x_1}$ nor $\mathbf{e}_{x_2}$, it is easy to see that this is generally not the case. It can be shown that $TV(\Pi_h\rho) = TV_2(\Pi_h\rho) \le TV_2(\rho)$, and therefore traditional perimeter methods converge to ($\mathbb{P}$) furnished with the anisotropic taxicab perimeter [5]. As shown in Fig. 1 the anisotropy for TV_m is much weaker for higher m, and in addition, if $\kappa = h_2/h_1$, one can, using the techniques in [8], prove the approximation property

$$TV_{m,h}(\Pi_h\rho) \le TV_m(\rho), \quad (m = 4, 8). \tag{4}$$

This inequality should be possible to generalize to non-smooth functions by approximation arguments, cf. Lemma 3.1 in [5]. However, the complete proofs for TV_m, $m > 2$, are still to be done.

Let ρ be a piecewise constant function. The formula for $m = 4$ reads

$$TV_{4,h}(\rho)/c_4 = \sum_{j=0}^{n_2}\sum_{i=1}^{n_1} h_2|\rho_{ij} - \rho_{i-1,j}| + \sum_{j=1}^{n_2}\sum_{i=0}^{n_1} h_1|\rho_{ij} - \rho_{i,j-1}|$$
$$+ \sum_{j=0}^{n_2-1}\sum_{i=0}^{n_1-1} \frac{h_1 h_2}{h}|\rho_{ij} - \rho_{i+1,j+1}| + \sum_{j=0}^{n_2-1}\sum_{i=1}^{n_1} \frac{h_1 h_2}{h}|\rho_{ij} - \rho_{i-1,j+1}|, \quad (5)$$

where $h = \sqrt{h_1^2 + h_2^2}$, and for $m = 8$,

$$TV_{8,h}(\rho)/c_8 = TV_{4,h}(\rho)/c_4 + \sum_{j=0}^{n_2-1}\sum_{i=2}^{n_1} \frac{h_1 h_2}{\sqrt{4h_1^2 + h_2^2}}|\rho_{ij} - \rho_{i-2,j+1}| + \sum_{j=1}^{n_2}\sum_{i=2}^{n_1} \frac{h_1 h_2}{\sqrt{4h_1^2 + h_2^2}}|\rho_{ij} - \rho_{i-2,j-1}|$$
$$+ \sum_{j=2}^{n_2}\sum_{i=1}^{n_1} \frac{h_1 h_2}{\sqrt{h_1^2 + 4h_2^2}}|\rho_{ij} - \rho_{i-1,j-2}| + \sum_{j=2}^{n_2}\sum_{i=0}^{n_1-1} \frac{h_1 h_2}{\sqrt{h_1^2 + 4h_2^2}}|\rho_{ij} - \rho_{i+1,j-2}|. \quad (6)$$

5. Numerical Examples

In order to compare the perimeter measures, the theoretical study is followed by two numerical implementations of the different perimeter measures. This implementation has been realized in two software programs based on two different approaches of topology optimization. The first approach [9] is the "classical" topology optimization approach of continuum structures in which the density is allowed to vary continuously from void to solid. The second approach is based on a pure discrete valued optimization [2,10] in which one considers only the solid and a very low density material. In both programs the solution procedure relies on the mathematical programming approach also called sequential convex programming. The initial implicit problems are replaced with a sequence of explicit, convex and separable subproblems based on approximation schemes. Then each of these subproblems is solved in the dual space, with continuous or discrete mathematical programming algorithms.

Cantilever Beam

In order to show the advantages of the proposed less anisotropic measures of perimeter, we consider first a benchmark that is a variant of the classical Michell benchmark (Fig. 2). The difficulty of the problem

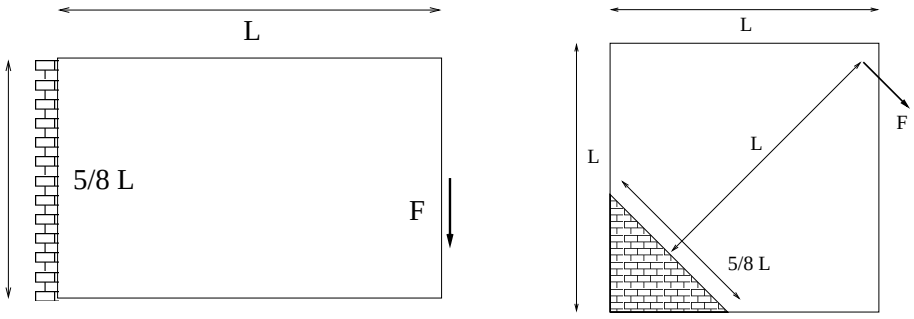

Figure 2: Short cantilever beam problem and its rotated counterpart

comes from the 45 degrees rotation of the mesh with respect to the directions of the supports and of the load. The domain is discretized in 3600 square finite elements. A discrete valued optimization is performed. The first solution (shown to the left in Fig. 3) uses the TV_2 measure which favours the presence of structural edges that are parallel to the mesh direction. In a second stage a better solution is reached with the new TV_4 measure (mid picture of Fig. 3). Its compliance is smaller and the internal structural members are nearly perpendicular to each other. Thus the structural topology of the TV_4 solution is closer to the theoretical and numerical solutions known from literature. The optimization has also been performed with a refined mesh composed of 8100 elements while keeping the same bound on the TV_4 perimeter (to the right in Fig. 3).

It was suggested originally in [9] that no additional strategy to alleviate the checkerboards is necessary when the perimeter bound is used. The checkerboards fade away from the solution for a sufficiently bounded perimeter, which is clearly illustrated in Fig. 4. The illustration problem is based on a continuum topology optimization with a low penalization of intermediate densities (exponent $p = 1.6$) which allows large composite zones in the design. The checkerboards are massively present when one does not constrain the

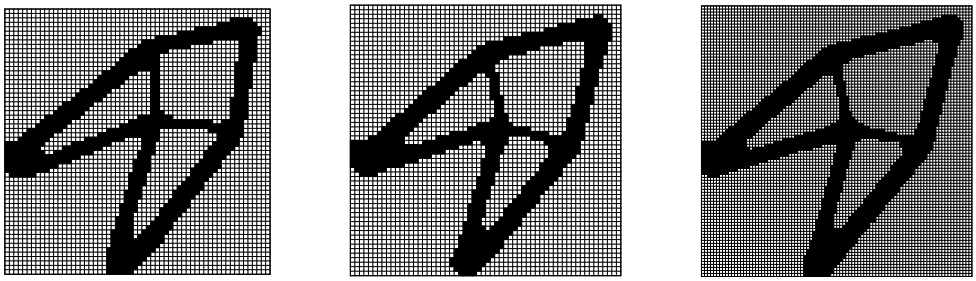

Figure 3: Solutions with discrete approach: TV_2 and TV_4 for coarse mesh, and TV_4 for fine mesh

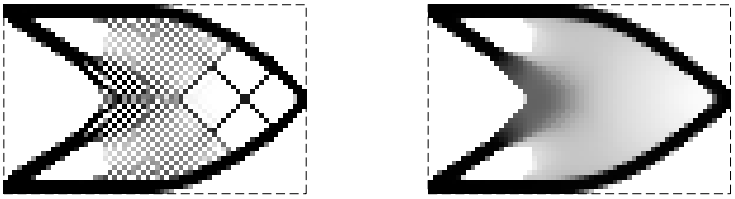

Figure 4: Solutions with continuous approach: No TV-bound, and $TV_4(\rho) \leq 90$

perimeter (as shown to the left in Fig. 4). They fade away progressively when the perimeter restriction becomes more and more restricting and they disappear totally for a bound of $TV_4 \leq 90$ (to the right in Fig. 4).

Industrial Benchmark

This application is based on an industrial benchmark proposed by the french steel maker SOLLAC. Topology optimization is used to design a pillar that supports crash barriers which are placed alongside roads and bridges. As the barrier volume is not part of the design, the pillar takes place in the remaining L-shaped part (Fig. 5). A pressure distribution modelling a car crash is applied on its upper part. The design

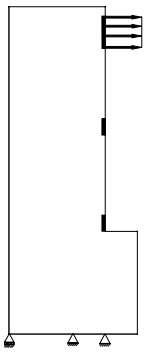

Figure 5: Geometry of the design domain and boundary conditions

domain is discretized by a regular mesh of 102 by 40 finite elements. Material data are given by steel. The volume bound is set to 25 percents. In this application, the perimeter constraint allows us to reduce the manufacturing complexity.

At first we consider the continuous variable approach. Optimal material distributions have been produced with the three proposed perimeter measures (see Fig. 6). We have grouped results that have been generated with different TV_m measures and different bounds $\overline{P}$, but that have the same topology. From a comparison of density maps, one can observe the influence of the measure upon the geometrical details (circled for easiness). As predicted by the theoretical study, TV_2 favors the directions along coordinate axes (horizontal

and vertical directions) whereas the quasi-isotropy property of TV_4 and TV_8 leads to introduce inclined lines and curves. The conclusions that can be deduced from these numerical experiments match perfectly with the theoretical conjectures of the first part.

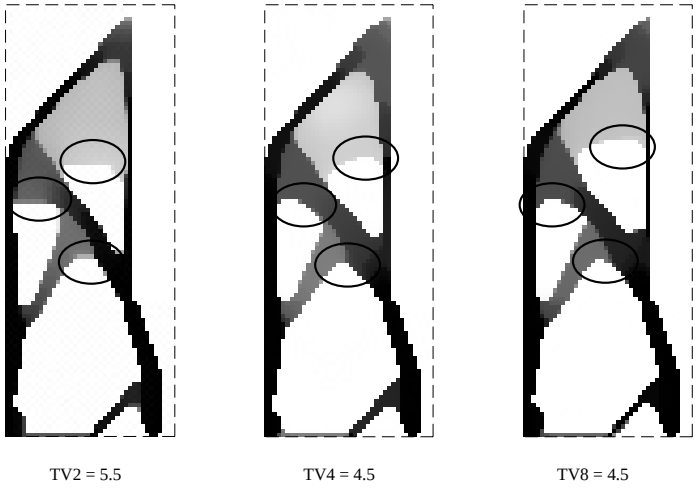

Figure 6: Comparison of TV_2, TV_4 and TV_8

Remarks

As a first remark we can underline the practical difficulty to find similar topologies with the different TV_m measures because they do not have the same numerical values and no relationship is available to relate them. We just know the ordering relationship $TV_8 \leq TV_4 \leq TV_2$. For precise numerical connection between the different $\overline{P}$-values, we had to proceed by trials and errors until we got similar topologies. This is not very convenient for industrial applications.

As a second remark we observed that the TV_4 measure is easier to control than the TV_2 perimeter from a numerical point of view. From previous study of the perimeter we know that the TV_2 measure is generally difficult to manage in the numerical procedure. It usually leads to a lot of constraint violations and we have to select quite "careful" optimization procedures based on a small move-limits strategy and small trust region approximations. As explained in [3], a special procedure has been tailored for the TV_2 perimeter

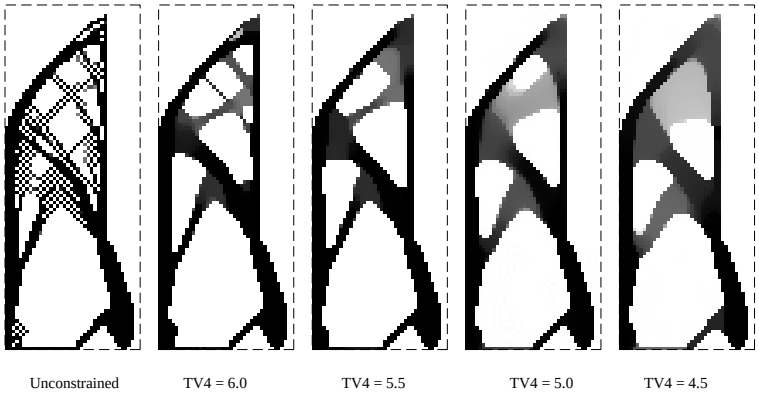

Figure 7: Results obtained with different bounds on TV_4 - continuous approach

constrained problems. When the same strategy is used for TV_4, the solution procedure gains in efficiency, reliability and stability. We interpret this observation as the result of the better quality of the perimeter measure, in which the influence of the whole neighborhood around each element is considered. This good quality acts also on the ability to control the topology complexity while playing with the perimeter bound. The controllability of the quasi-isotropic measure TV_4 is high as illustrated in Figs 7 and 8, for the continuous and the discrete approaches respectively. Moreover, as it is suggested in the theoretical part, checkerboards

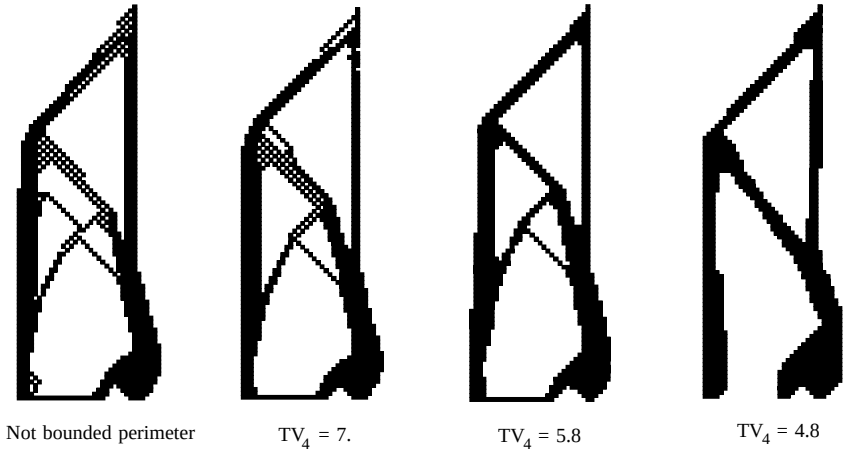

Figure 8: Results obtained with different bounds on TV_4 - discrete approach

fade out for a sufficiently low perimeter. The checkerboard patterns of the unconstrained distribution of Figs 7 and 8 disappear quite immediately with a perimeter bound. This is true with any TV_m measure, but the controllability of TV_4 makes it easier.

6. Conclusions

This numerical application has illustrated three aspects of the perimeter approach:

- the solution tends to be rotationally mesh-independent when using less anisotropic perimeter measures;
- the bound on the perimeter helps to reach a solution with the same topology while mesh-refinement;
- the checkerboards fade away for sufficiently bounded perimeter.

7. Acknowledgements

This work was financially supported by the Swedish Research Council for Engineering Sciences TFR and the National Network in Applied Mathematics NTM (for the first author), and by the BRITE-EURAM project COMPOPT (contract BRPR-CT96-0332 of the European Community) (for the two last authors).

8. References

[1] Haber, R.B., Bendsøe, M.P., and Jog, C. (1996). A new Approach to Variable-Topology Shape Design Using a Constraint on the Perimeter. *Structural Optimization*, **11**, 1–12.

[2] Beckers, M. (1999). Topology Optimization Using a Dual Method with Discrete Variables. *Structural Optimization*, **17**, 14–24.

[3] Duysinx, P. (1997). Layout Optimization: A Mathematical Programming Approach, DCAMM Report No. 540, Technical University of Denmark.

[4] Ambrosio, L. and Buttazzo, G. (1993). An Optimal Design Problem with Perimeter Penalization. *Calculus of Variations*, **1**, 55–69.

[5] Petersson, J. (1999). Some Convergence Results in Perimeter–Controlled Topology Optimization. *Computer Methods in Applied Mechanics and Engineering*, **171**, 123–140.

[6] Chambolle, A. (1995). Image Segmentation by Variational Methods: Mumford and Shah Functional and the Discrete Approximations. *SIAM Journal on Applied Mathematics*, **55**, 827–863.

[7] Chambolle, A. (1997). Finite Differences Discretizations of the Mumford-Shah Functional, CNRS Report No. 9727, Université de Paris Dauphine.

[8] Petersson, J. (1999). Numerical Instabilities in Topology Design Computations. *Progress in Industrial Mathematics at ECMI 98*, edited by Arkeryd, L., Bergh, J., Brenner, P., and Pettersson, R., Teubner, Karlsruhe, 431–438.

[9] Duysinx, P. (1996). Optimisation Topologique : du Milieu Continu à la Structure Élastique, Ph. D. thesis, University of Liège.

[10] Beckers, M. (1997). Optimisation de Structures en Variables Discrétes, Ph. D. thesis, Collection des Publications de la Faculté des Sciences Appliquées 181, University of Liège.